IKR Journal of Engineering and Technology (IKRJET)

Journal homepage: https://ikrpublishers.com/ikrjet/ Volume-1, Issue-2 (September-October) 2025



Transformation of Goethite into Hematite: Mechanisms, Technological Routes, and Industrial Applications—A Critical Review (2020–2025)

Antonio Clareti Pereira*

PhD in Chemical Engineering, Federal University of Minas Gerais – UFMG, Department of Chemical Engineering, Belo Horizonte – MG – Brazil

DOI:10.5281/zenodo.17265013

ARTICLE INFO

Article history: Received: 26-09-2025 Accepted: 01-10-2025 Available online: 04-10-2025

Copyright©2025 The Author(s): This is an open-access article distributed under the terms of the Creative Commons Attribution 4.0 International License (CC BY-NC) which permits unrestricted use, distribution, and reproduction in any medium for non-commercial use provided the original author and source are credited.

Citation: Pereira, A. C. (2025). Transformation of Goethite into Hematite: Mechanisms, Technological Routes, and Industrial Applications—A Critical Review (2020–2025). *IKR Journal of Engineering and Technology (IKRJET)*, 1(2), 68-85.



ABSTRACT

Original research paper

Goethite (\alpha-FeOOH) is one of the most common iron oxyhydroxides found in lateritic iron ores, bauxite residues, and sludges from hydrometallurgical processes. It presents significant challenges due to its high structural water content, fine particle size, and low thermal stability, which affect mineral processing, filtration, and metallurgical operations. Converting goethite into hematite (α-Fe₂O₃) or other dehydrated iron oxides is crucial for enhancing material handling, improving process efficiency, and facilitating the production of high-value products, such as iron ore pellets and pigments. This review provides a comprehensive analysis of the mechanisms, thermodynamics, and kinetics that govern the dehydration of goethite through thermal, hydrometallurgical, and hybrid methods. It highlights recent advances (2020–2025) in process technologies, such as low-carbon heating techniques, controlled precipitation, and integrated circular economy strategies for residue valorization. Characterization methods, such as X-ray diffraction (XRD), Mössbauer spectroscopy, and thermogravimetric analysis (TGA), are examined for their roles in monitoring phase transformations. The review also critically assesses industrial applications, process optimization strategies, and future perspectives, emphasizing the importance of goethite transformation for sustainable iron production and waste management.

Keywords: Goethite, Hematite, Dehydroxylation, Iron ore, Thermal transformation, Waste valorization.

*Corresponding author: Antonio Clareti Pereira

PhD in Chemical Engineering, Federal University of Minas Gerais – UFMG, Department of Chemical Engineering, Belo

Horizonte-MG-Brazil

1. Introduction

1.1. Natural occurrence of goethite and its importance in industry

Goethite (α -FeOOH) is a prevalent iron oxyhydroxide that forms in oxidizing, humid environments. It appears in lateritic profiles, soils, and industrial waste like red mud from the Bayer process, nickel laterite tailings, and limonitic ores [1,2]. It can develop through the precipitation of ferric iron in aqueous systems or by transforming poorly crystalline precursors such as ferrihydrite at ambient or moderate temperatures and neutral to slightly acidic pH [3]. The mineral usually has small particles and contains high levels of

structural (bound) water. It exhibits various shapes—from needle-like and fibrous to more massive aggregates—and often shows significant substitution by elements like Al and Si, which influence its thermal stability and transformation characteristics [4,5].

In high-goethite iron ores, also known as goethitic or goethite-rich ores, goethite often constitutes the main iron-bearing phase. These ores are typically found in lateritic limonite deposits, weathered crusts, and red mud waste. Their beneficiation presents particular challenges: the high water content increases moisture and energy demand for drying; fine particles and intergrowths with gangue complicate separation; impurities and substitutions alter dehydration and

dehydroxylation temperatures; and the hydroxyl-rich structure causes instability under heat, resulting in volume changes, microcracks, and reduced mechanical strength [5,6].

1.2. Issues associated with elevated goethite levels in iron ores

Minerals containing high levels of goethite pose several technical challenges..

- High moisture or combined water content demands significant energy for drying, resulting in increased transportation and handling costs [11].
- Thermal instability: Goethite begins to lose hydroxyl groups (dehydroxylation) at relatively low temperatures, typically around 250-400 °C, depending on factors such as substitutions and particle size. This process causes structural changes, increases porosity, forms microcracks, and weakens processes like sintering, pelletizing, filtration, and handling [12, 13].
- Filtration, separation, and handling issues: Small particle size and water retention reduce efficiency. Additionally, fluidization of filtration and solid-liquid separation, along with magnetic or gravity separation, is limited because goethite is only weakly magnetic and often closely linked with gangue. Impurities such as Al, Si, and P also affect its behavior [2, 7].
- Downstream process inefficiencies include increased energy use during drying and phase changes, potential weak strength or permeability in pellets or sinters, and possible impacts on pigment and color properties. Additionally, waste and residue utilization often face challenges with low iron content and large quantities of tailings [14, 16].

For example, a recent study on the magnetization roasting of red mud/limonite-type residues identified dehydration and the conversion of goethite into hematite as essential steps before transforming into magnetite through magnetic separation. The activation energies of these processes are affected by impurity levels and the atmosphere [8]. Another recent investigation into low-grade iron ore fines found that optimal conversion of goethite to hematite (or other magnetic phases) depends on carefully controlling roasting temperature—typically around 650-700 °C—and the atmosphere. This careful control maximizes recovery and prevents over-reduction [9].

1.3. Significance of transforming goethite into hematite and dehydrated oxides

Converting goethite into hematite or other dehydrated oxides provides various industrial benefits.

- Hematite (α-Fe₂O₃) offers greater thermal stability, remaining structurally and thermally stable at higher temperatures; after dehydroxylation, it becomes less prone to structural collapse.
- Enhanced filtering, density, and mechanical properties:
 Removing structural water and hydroxyl groups reduces

- volume, increases density, and boosts strength; lower porosity improves filtration and handling; and the material exhibits more consistent behavior during pelletizing, sintering, or direct reduction.
- Improved performance in metallurgical and chemical uses includes hematite's superior results in pigment production (color stability, purity), ironmaking processes (blast furnace, direct reduction, hydrogen routes), and residue valorization (red mud, limonite). It achieves this by boosting iron content, reducing waste, and promoting circular economy practices.

1.4. Objectives of this review

Given the renewed interest from 2020 to 2025 in sustainable iron production, residue valorization, low-carbon technologies, and processing lower-grade or goethitic ores, this review aims to:

- Critically examine the processes that convert goethite into hematite or other dehydrated iron oxides. Include dehydroxylation, structural transformations, phase nucleation, formation of intermediates, kinetics, and the role of substitutions.
- Compare and analyze the technological pathways thermal, hydrometallurgical, and hybrid—that have been developed or demonstrated from 2020 to 2025, focusing on energy usage, environmental effects, and scalability.
- Evaluate the techniques employed in these studies—such
 as XRD, Mössbauer spectroscopy, TG/DTA, and
 microscopy—and determine how they assist in
 monitoring and controlling the process.
- 4. Identify gaps, challenges, and future directions in the beneficiation of goethitic ores, especially those with high structural water, fine particles, impurity content, and where low-carbon or circular economy constraints are significant.

2. Methodology for Conducting Literature Review

This review adheres to a well-defined protocol based on PRISMA (Preferred Reporting Items for Systematic Reviews and Meta-Analyses) guidelines [10].

Search strategy:

Searches were performed in Scopus, Web of Science, and Google Scholar using keywords like goethite, hematite, dehydroxylation, iron oxyhydroxide transformation, goethite-rich ore beneficiation, Algoethite thermal conversion, and laterite goethite transformation. A date filter was applied for studies published from 2020 to 2025, inclusive.

• Inclusion Criteria:

- a. Studies were published between 2020 and 2025.
- b. Peer-reviewed journal articles, dissertations, or theses with full text available.

- c. Reporting original experimental or technological data on the transformation of goethite into hematite or other dehydrated oxides, as well as beneficiation of goethitic ores involving phase changes.
- d. Provide a valid DOI or a working URL.

• Exclusion Criteria:

- a. Studies are reviewed prior to 2020 unless they are foundational for context. .
- Reviews should incorporate new experimental data unless they already offer essential quantitative comparisons.
- c. Include only studies published in English unless they are translated and fully available.
- d. Studies that involve goethite but do not characterize transformation details such as phase changes, kinetics, or structural and morphological data.

• PRISMA flow process:

The PRISMA flow diagram (Figure 1) illustrates the study selection process for this review. Initially, 612 studies were identified via database searches. After screening titles and abstracts, 198 studies were removed due to duplication or irrelevance, leaving 414 studies for full-text evaluation. Upon assessing eligibility, 331 studies were excluded for not meeting specific inclusion criteria, resulting in 83 studies included in the systematic review. This approach promotes transparency, reproducibility, and adherence to PRISMA 2020 guidelines [1, 9].

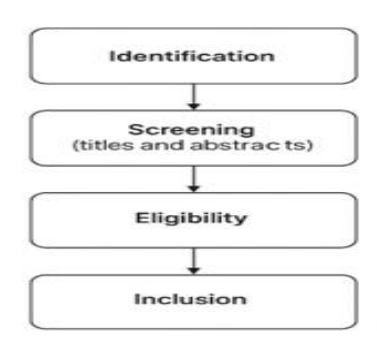


Figure 1. PRISMA flow process

3. Theoretical Background

3.1. Crystal structure of goethite and its comparison with hematite

Goethite (α-FeOOH) has an orthorhombic structure (space group Pnma, no. 62) composed of slightly distorted FeO₆ octahedra that share edges, forming double chains aligned parallel to the c-axis (see Figure 2). These chains are connected by corner sharing, creating one-dimensional tunnels within the framework. Hydroxyl groups occupy specific octahedral sites and form a strong, directional hydrogen-bond network that links neighboring chains and lines of these tunnels. Molecular H₂O mainly associates with surfaces, defects, or nanoporosity, rather than the bulk lattice

itself [17–19]. This topology introduces noticeable anisotropy, such as acicular growth along the [001] direction and affects the vibrational signatures of the OH sublattice observed in Raman/IR spectroscopy [17]. Isomorphic substitutions, mainly with Al and to a lesser extent with Ga, can modify lattice parameters, particle aspect ratio, and surface site distribution without altering the core Pnma structure. Recent DFT and experimental research indicate that these substitutions cause only minor structural changes in goethite compared to ferrihydrite [19, 23].

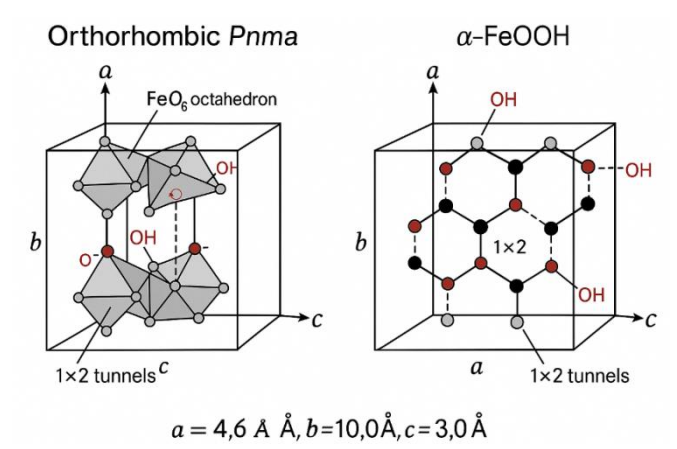


Figure 2. Crystal structure of goethite

Hematite (α-Fe₂O₃) has a corundum-type trigonal (rhombohedral) lattice (space group R-3c, no. 167), featuring a close-packed oxygen sublattice with Fe³⁺ ions in octahedral sites arranged in hexagonally stacked layers (see Figure 3). It is fully dehydroxylated, lacking structural OH groups and hydrogen-bonded channels [21]. When goethite is heated in a topotactic or reconstructive manner, dehydroxylation and lattice reorganizations create hematite or vacancy-rich "hydrohematite/protohematite" intermediates, where residual protons and cation vacancies may remain depending on thermal history, particle size, and chemistry [20–22].

These crystallographic differences (Figure 3)—orthorhombic OH-bearing tunnels in goethite compared to dense, OH-free corundum layers in hematite—cause significant variations in thermal stability, density, filtrability, and the propensity of goethite-rich feeds crack, micro-porate, and weaken when heated. These factors directly impact sintering, pelletizing, and pigment performance (discussed in later sections) [20–22].

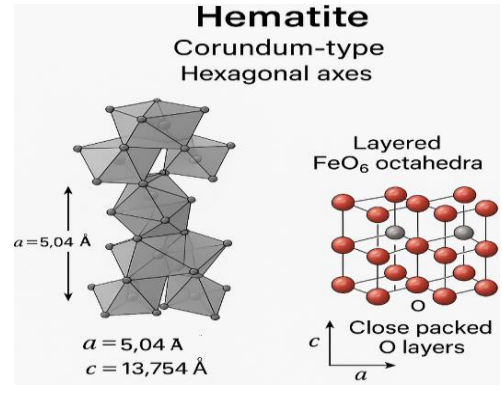


Figure 3. Crystal structure of hematite.

Table 1 summarizes the main crystallographic features of goethite and hematite, emphasizing the orthorhombic OH-bearing structure of α -FeOOH in contrast to the OH-free corundum-type lattice of α -Fe₂O₃. It also discusses the implications for thermal properties and processing.

Table 1.Crystal-chemistry summary (room temperature, representative values)

Parameter	Goethite (α-FeOOH)	Hematite (α-Fe ₂ O ₃)
Crystal system / space group	Orthorhombic, Pnma (often reported as Pbnm)	Trigonal (hexagonal setting), R-3c
Lattice constants (Å)	a≈4.61, b≈9.96, c≈3.02 (Pnma); equivalent setting frequently reported as a≈9.91, b≈3.01, c≈4.58 (axis relabeling)	a=b≈5.0356, c≈13.7489
Fe coordination & connectivity	FeO ₆ octahedra in double chains $\rightarrow 1 \times 2$ tunnels lined by OH; H-bonded network along tunnels	Distorted FeO ₆ octahedra in layered corundum framework; no structural OH in stoichiometric hematite
Representative Fe–O distances (Å)	~1.97–1.98 (EXAFS, average octahedral Fe–O)	~1.94 and ~2.11–2.12 (two distinct Fe–O within distorted octahedra)
OH / H-bonding signatures	Structural OH; Raman/IR O–H stretching bands in ~3100–3600 cm ⁻¹ region; H-bonding governs band positions and width	Nominally absent; vacancy-bearing hydrohematite shows additional OH-related bands and lattice expansion
Thermal behavior (dehydroxylation)	Dehydroxylations to hematite typically from ~250–400 °C (composition/size dependent)	Stable to higher T; no dehydroxylation (but hydrohematite can dehydroxylation/anneal toward stoichiometric hematite)

Notes and sources.• Goethite lattice parameters and orthorhombic setting (Pnma/Pbnm) and α -FeOOH tunnels: Senamart*et al.* 2022 (RSC Adv.) and MDPI *Materials* 2022 (axis relabeling in Pnma model).

- Hematite space group and lattice constants; Fe–O distances in distorted octahedra: Huang & Cheng 2024 (Sci Rep.).
- Average Fe–O in goethite from Fe K-edge EXAFS: Senamart *et al.* 2022 (RSC Adv.).
- Goethite OH vibrational signatures and assignment: Abrashev*et al.* 2020 (J Appl Phys.).
- Hydrohematite (vacancy-bearing α -Fe₂O₃ with structural water): Chen *et al.* 2021 (Geology).
- Goethite dehydroxylation temperature window (particle size/substitution dependent): Zhou *et al.* 2022 (RSC Adv.).

Values are based on recent experimental and DFT studies, with minor differences arising from temperature, particle size, and isomorphic substitutions, particularly involving Al/Ga. Goethite has an orthorhombic Pnma structure, featuring FeO₆ octahedra that form 1 × 2 tunnels lined with structural OH groups. Hematite is trigonal (R-3c), similar to corundum, and is nearly anhydrous. Changes in OH content, Fe–O distances, and packing structure affect dehydroxylation temperatures, density, filtrability, and mechanical properties, which are essential for pelletizing and sintering [17–25].

3.2. Critical analysis — Why crystal structure matters in processing

Goethite has an orthorhombic, tunneled structure with structural OH groups that dehydroxylate at relatively low temperatures, releasing steam, causing microcracks, and creating temporary porosity. In contrast, hematite's close-packed corundum lattice (R-3c) is almost anhydrous and densifies without volatile release. These distinctions influence drying and preheating processes, heat—mass transfer, and defect formation during agglomeration and thermal upgrading. As a result, goethitic pellets require staged drying and gentler preheating to avoid spalling and strength reduction. In contrast, hematitic feeds can tolerate faster heating rates and achieve higher induration strength within similar thermal budgets [23–25, 28].

During sintering, the initial dehydroxylation of goethite enhances green-bed permeability and facilitates the formation of melting pathways. However, if heating is too intense or the melt volume is insufficient, the microcrack network can weaken the sinter's strength. Optimal blending or process control strategies that temporarily maintain permeability and prevent crack coalescence can consistently boost sinter yield. Recent pilot studies and modeling research explicitly link bed porosity changes, pressure drops, and coke consumption to the kinetics of goethite converting into hematite.

For pelletizing, surface hydroxylation on goethite promotes nucleation and binding. However, a high LOI raises energy use and may weaken microstructures unless preheating and hold times are optimized to fully dehydroxylate before load-bearing densification occurs. Micro-CT and in-melt studies reveal crack formation near the α-FeOOH breakdown zone, with sustained reduced strength unless thermal schedules are modified; hematite feeds display fewer defects under comparable conditions [28,32].

The structural pathway remains crucial during beneficiation by magnetization roasting or H₂ reduction.

Goethite transforms through hydro/hematite/proto-hematite intermediates containing vacancy/OH defects, facilitate diffusion routes and enable magnetite formation or H₂ reduction at lower temperatures compared to dense, wellcrystallized hematite of similar size—assuming cracking is managed. Recent industry-relevant research on magnetization roasting and H2-based reactors demonstrates lower initial temperatures and quicker conversions when using goethitic or limonitic feeds, improving Fe recovery at moderate temperatures and shorter durations [26-27]. Insights from time-resolved diffraction and vacancy-filling studies suggest that OH- and vacancy-rich intermediates affect both the reaction kinetics and the final mechanical strength; controlling these intermediates now provides opportunities to develop low-carbon processes such as H2 SMR and ZESTY [29–30, 26].

In pigment and specialty applications, the link between structure and shape is crucial. Hematite created through controlled precipitation and thermal conditions consistently exhibits specific size, shape, and color properties that are hard to replicate through dehydration, which often causes uncontrolled cracks. By adjusting pH and precipitants and preventing residual magnetite, it is possible to attain predictable Lab* responses and reduced oil absorption. These advantages are associated with corundum topology and the lack of structural OH.

Table 2. Enumerated transformation steps (R1–R4) for goethite–hematite–magnetite–iron pathways, including representative reactions, common temperature ranges, and gas/O₂ control strategies. Values are approximate and depend on particle size, isomorphic substitutions (e.g., Al), heating rate, and gas humidity. Controlling H_2O/H_2 (or CO_2/CO) is essential to select the direct Fe_3O_4 —Fe route (R3, \leq ~570 °C) or the wüstite-mediated route (R4, >~570 °C). Dehydroxylation (R1) should be finished before high-load densification to prevent microcrack-induced strength loss [12, 18, 26, 33, 35, 36, 40].

Table 2. Sequential Solid-State Transformations of Iron Oxides during Thermal Treatment

Transformation (R1–R4)	T (°C)	Gas /pO ₂
R1. Goethite \rightarrow Hematite 2 FeOOH (s) \rightarrow Fe ₂ O ₃ (s) + H ₂ O (g)	≈ 250400	Inert or oxidizing; remove H ₂ O
R2. Hematite \rightarrow Magnetite 3 Fe ₂ O ₃ (s) + H ₂ \rightarrow 2 Fe ₃ O ₄ (s) + H ₂ O (g) (or CO \rightarrow CO ₂)	≈ 350–700	Reducing (H ₂ /H ₂ O or CO/CO ₂)
R3. Magnetite \rightarrow Iron (direct) — Fe ₃ O ₄ (s) + 4 H ₂ \rightarrow 3 Fe (s) + 4 H ₂ O (g)	≥~500	Strongly reducing; low H ₂ O/H ₂
R4. Magnetite \rightarrow Wüstite \rightarrow Iron — Fe ₃ O ₄ + H ₂ \rightarrow 3 FeO + H ₂ O; FeO + H ₂ \rightarrow Fe + H ₂ O	>~570	Very low pO ₂ ; H ₂ /H ₂ O or CO/CO ₂ set FeO stability

Table 3 outlines the primary Fe-oxide transformation stages relevant to goethitic feeds. It details the gas atmosphere/oxygen potential, kinetic and structural effects, and processing implications for each step, supported by references [12, 18, 26, 29, 33, 35, 36, 40].

Table 3. Phase transformation steps for goethite-hematite-magnetite-iron during processing conditions.

Step	Gas atmosphere / oxygen potential	Kinetic/structural notes	Processing implications
Goethite →			
Hematite		OH loss \rightarrow vacancy generation;	Stage drying & preheat; complete
(dehydroxylation	Inert or oxidizing; water	transient porosity & microcracks;	dehydroxylation before high-load
)	removal critical	vacancy infilling during anneal	densification to avoid strength loss
Hematite \rightarrow	Reducing (H ₂ /H ₂ O or	Pore evolution governs rates; water	Tune H ₂ O/H ₂ (or CO ₂ /CO) and T; avoid
Magnetite	CO/CO ₂); pO ₂ and H ₂ O/H ₂	vapor suppresses $Fe_3O_4 \rightarrow Fe$;	excessive sintering; leverage faster
(reduction)	ratio control equilibrium	sintering at high T can slow kinetics	kinetics vs dense hematite
		Direct path favored at ≤~570 °C;	
Magnetite →	Strongly reducing; low	higher T may form FeO first,	Control moisture in gas; ensure adequate
Iron (direct)	H ₂ O/H ₂ (or CO ₂ /CO)	depending on gas	residence time; manage densification
Magnetite →			At high T, expect FeO stage; adjust
Wüstite → Iron	Very low pO ₂ ; H ₂ /H ₂ O or	FeO is transient; sintering can be	temperature and gas to avoid kinetic
(via FeO)	CO/CO ₂ set FeO stability	significant at higher T	bottlenecks

3.3. Thermodynamics and kinetics of goethite dehydroxylation

Balanced reactions and mechanistic notes

The main dehydration and dehydroxylation process is:

R1 (dehydroxylation): 2 FeOOH(s) → Fe₂O₃(s) + H₂O(g). This process usually occurs topotactically, involving transitions through proto- and hydrohematite with cation-vacancy ordering before forming stoichiometric hematite. The exact pathway depends on factors like particle size, crystallinity, and isomorphic substitutions such as Al or Ga [12, 18, 20, 38].

Thermodynamics (covering ΔH , ΔG , and the importance of water activity)

DSC/DTA consistently show endothermic dehydroxylation events for α -FeOOH. Recent high-temperature DSC studies indicate one or two endothermic peaks linked to R1, with individual enthalpies around 300–470 J g⁻¹ (varying with sample and grain size) [44]. When converted to per mole of FeOOH, these values approximate 26–41 kJ mol⁻¹ per FeOOH for a single event, noting that some samples display split peaks due to overlapping defectannealing and OH-loss processes [44].

From a basic equilibrium standpoint for R1 (where the solid activities are approximately 1), K is roughly equivalent to $p(H_2O)$, so ln K equals $-\Delta G^{\circ}(T)/RT$, which is also ln $p(H_2O)$. Consequently, higher water vapor pressures push the equilibrium toward goethite, requiring higher temperatures for complete dehydroxylation; conversely, lower $p(H_2O)$ levels (such as under vacuum) lower the energy barrier and shorten the time to achieve completion at a given temperature [41,42]. In ultra-high vacuum conditions, dehydration starts much earlier than under ambient conditions. At moderate vacuum, the temperature range stays nearly the same, but the residence time drops sharply— for example, from 24 hours to about 1 hour at 300 °C [42].

Kinetics (Ea and key factors affecting rate)

Non-isothermal analyses like isoconversional/FWO and Kissinger methods evaluate apparent activation energies, which can vary significantly based on ore matrix, crystallinity, and particle size. Recent inert-condition studies on ore-specific samples show that the stage-dependent Ea for goethite decomposition ranges from about 45 to 135 kJ mol⁻¹, depending on whether the process is chemically controlled or diffusion-limited [43]. Values outside this range occur when pore-forming or annealing processes are combined with OH loss, or when substitutional cations such as Al stabilize the OH structure [4, 12, 20]. Water vapor in the sweep gas slows the reaction by inhibiting products and reducing the chemical potential gradient for H2O removal, while drier or vacuum conditions accelerate devolatilization and increase porosity [42]. Operando/in-situ XRD indicates that vacancy filling and ordering toward stoichiometric hematite continue after the main endothermic OH-loss, so isothermal holds above the dehydroxylation peak are often required to complete defect annealing [38].

Impacts of T-p-gas on processing windows

- Temperature: R1 typically starts between 250 and 400 °C, depending on size, defects, and substitutions; some smaller or strained populations and inclusions exhibit onset below 300 °C with narrow conversion ranges [12,45].
- Lowering p(H₂O), like in high vacuum conditions, significantly shortens the necessary hold times at a specific temperature; in industrial settings, this results in quicker pre-heating and drying or increased bed permeability during pre-induration [42].
- Gas composition: Inert or mildly oxidizing gases facilitate clean OH removal; however, any reducing component may cause partial Fe³⁺ to Fe²⁺ reduction at higher temperatures, leading to magnetite or wüstite formation. While this occurs outside the dehydroxylation window, it is relevant for coupled DR processes [26, 33, 35, 40].
- Microstructure: R1 generates temporary porosity and microcracks that can enhance downstream reducibility. However, without proper annealing using a controlled ramp, these features might weaken pellets or sinters. Careful sequencing of drying, dehydroxylation, and densification processes helps minimize strength loss [12, 18, 31, 33].

4. Transformation mechanisms

4.1. Solid-solid mechanisms

When heated under controlled conditions, goethite (α -FeOOH) directly dehydroxylates into hematite (α -Fe₂O₃) through a process involving limited long-range material transport (R1). Hematite nuclei tend to form at defect-rich areas, such as those caused by the removal of OH vacancies. These nuclei then grow and merge along preferred orientations, often maintaining the original shape via a topotactic or pseudomorphic process. The process of filling and ordering vacancies continues during short anneals just above the dehydroxylation temperature, which reinforces the lattice structure and reduces temporary porosity (see §4.3) [12, 18, 38].

Under low $p(H_2O)$ conditions, such as vacuum, the resistance to water removal is reduced, which accelerates dehydroxylation and results in a more porous, nanoparticle-like hematite—advantageous when higher reducibility is required [42]. Recent crystallographic research also shows inherited texture along the goethite \rightarrow hematite \rightarrow ferrite pathway, indicating that oriented precursors influence the magnetic and crystal anisotropy of the final product; this supports the idea that nucleation, growth, and coalescence occur under topotactic control [51]. Ab-initio studies of similar Fe oxyhydroxides suggest that short-range cation

rearrangements can lower the energy barrier for solid-state transformations, explaining why nanoscale, defective goethite converts at lower temperatures compared to larger, well-crystallized forms [52].

Figure 4 contrasts the energy landscape of the solid-solid dehydroxylation pathway (R1) with that of a dissolution-precipitation process. It highlights the nucleation \rightarrow growth \rightarrow coalescence sequence described later and the alternative pathway detailed in §4.2.

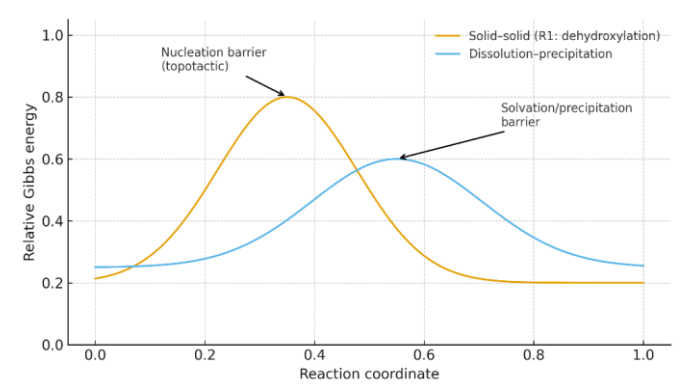


Figure 4. Energy profiles (solid–solid vs dissolution–precipitation

Figure 5 presents Arrhenius plots (ln k vs 1/T) for goethite dehydroxylation (R1), showing how apparent activation energies (approximately 60, 90, 120 kJ mol⁻¹) relate to p(H₂O), particle size, and defects. Lower p(H₂O) or vacuum conditions increase ln k by reducing product inhibition. Typically, coarser or more ordered grains exhibit higher Ea. The schematic indicates common ranges; see references [41–44] and prior studies [4, 12, 18].

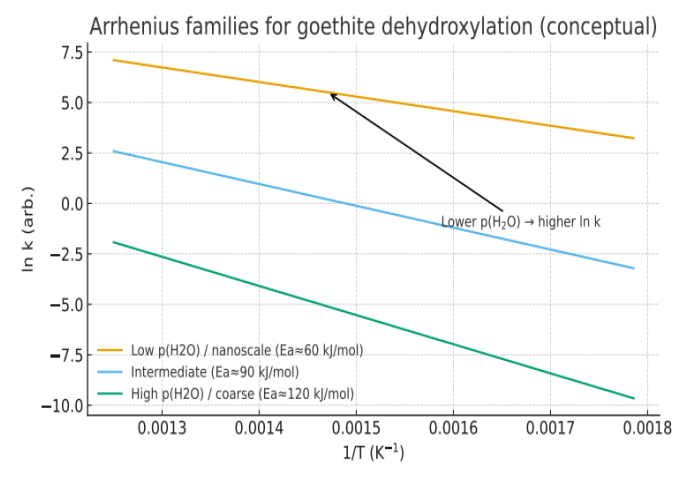


Figure 5. Arrhenius families for R1 (ln k vs 1/T)

4.2. Dissolution-precipitation process

In aqueous environments, especially at extreme pH levels or when Fe(II) is present, goethite-hematite transformations mainly occur through the dissolution of the original mineral followed by the reprecipitation of the new phase. At very high pH levels (\geq 13), ferrihydrite dissolves quickly and reprecipitates as goethite, showing a strong dependence on pH [10]. Fe(II) accelerates this conversion by

facilitating electron transfer at goethite surfaces and guiding nucleation, thus speeding up the transformation in mixed mineral assemblages [46]. In systems like acid mine drainage, schwertmannite and jarosite typically convert into goethite and, upon heating, transform into hematite. The specific pathway and rate vary depending on pH, temperature, and coprecipitated oxyanions such as AsO₄²⁻, CrO₄²⁻, and MoO₄²⁻, which also affect contaminant mobility [47–49]. Liquid-phase TEM studies and kinetic modeling reveal that nanoscale dissolution of goethite is anisotropic and that local redox and acid—base conditions govern dissolution and reprecipitation, shedding light on the heterogeneous textures seen in ores and residues [50].

Figure 6 shows a conceptual pH–rate envelope for the solution-mediated pathway. At very high pH levels (≥13), ferrihydrite dissolves and quickly reprecipitates as goethite [10]; under acidic, AMD-like conditions, schwertmannite and jarosite transform into goethite, with oxyanions like SO₄^{2−}, AsO₄^{3−}, and CrO₄^{2−} influencing both pathways and their rates [47–49]. This schematic serves as a process guide—quantitative kinetics depend on temperature, Fe(II) activity, and ionic strength, as explained in §5.1 [46,53].

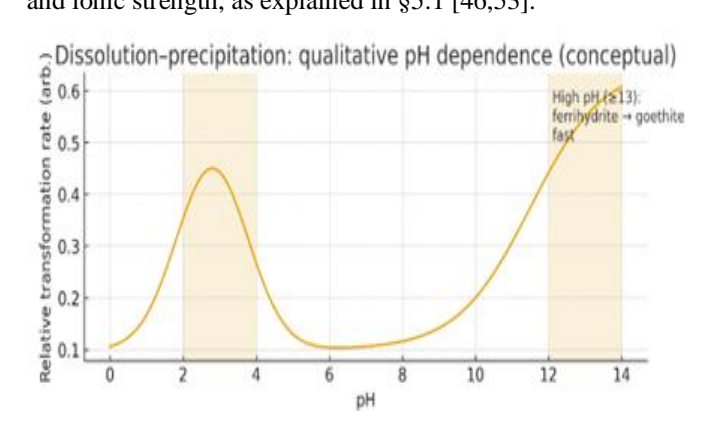


Figure 6. Qualitative pH–rate map (dissolution–precipitation):

4.3. Factors that influence the transformation

Particle size and crystallinity influence goethite behavior: smaller, defect-rich grains dehydroxylate at lower temperatures, creating temporary porosity; larger, wellcrystallized particles need longer or higher-temperature treatments and tend to sinter (see §4.3) [18, 38, 42]. Impurities and substitutions like Al, Si, and P affect goethite stability, shifting R1, and impact porosity and the goethite/hematite distribution, which influences filtrability and strength [12, 20]. Phosphate and other oxyanions can slow dissolution and alter dissolution-precipitation pathways; field data indicate that phosphate contact with soil strongly ferrihydrite/lepidocrocite. Process atmospheres include air, H2, CO, and N2. In inert or oxidizing conditions, R1 is driven by water removal; in reducing environments, the Fe₂O₃ to Fe₃O₄ or Fe transformation depends on pO₂ and H₂O/H₂ (or CO₂/CO) ratios (see §4.2). Thus, staging drying and dehydroxylation is essential to avoid microcracks before densification [26, 33, 35, 36, 40]. Using vacuum reduces

water content, shortens R1 hold times, and increases microstructural openness [42].

Process atmosphere includes air, H_2 , CO, and N_2 . In inert and oxidizing conditions, R1 is driven by the removal of H_2O ; in reducing environments, the transformations of Fe_2O_3 to Fe_3O_4 or Fe are controlled by pO_2 and the ratios of H_2O/H_2 or CO_2/CO (see §4.2). As a result, drying and dehydroxylation should be performed in stages to avoid microcracking prior to densification [26, 33, 35, 36, 40]. Using a vacuum reduces a (H_2O) and shortens the hold times for R1, while also increasing the openness of the microstructure [42].

5. Technological routes

5.1. Thermal processes such as drying, preheating, and calcination

Goethitic feeds, such as ores, bauxitic residues, and laterites, are typically conditioned by staged drying at temperatures of up to 150–200 °C to eliminate free moisture. This is followed by controlled dehydroxylationat temperatures ranging from 250 to 400 °C to transform FeOOH into Fe₂O₃, and finally, an annealing process at approximately 400–700 °C to reduce transient porosity and enhance the strength of the agglomerate. The main equipment used includes rotary kilns, grate–kiln systems, and belt furnaces, chosen for their capacity and ability to regulate residence time. Conversely, fluidized beds offer superior heat and mass transfer for fine feeds, enabling more precise control of pO₂.

Microwave heating is increasingly adopted for predrying or pre-heating due to its volumetric and selective heating abilities, which can reduce processing times and energy consumption when the dielectric properties are suitable. In all cases, managing gas composition and H_2O partial pressure is crucial to prevent re-hydroxylation and

undesired reduction or sintering. Optional magnetization roasting (350–650 °C in H_2/CO) can be performed if magnetite is required for beneficiation or DRI production. The primary operational goals include removing bonded water before high-load densification, preventing oversintering (which reduces the reactive surface area), and controlling the atmosphere—utilizing inert or oxidizing gases for R1, and reducing conditions for optional R2. [11, 23–25, 31–32, 40, 56, 60–62].

Industrial examples.

- Iron-ore sintering and pelletizing plants employ drying, preheating, and roasting processes customized based on ore LOI and goethite levels; maintaining bed permeability and pore structure is crucial for efficient heat transfer and mechanical robustness. [23–25, 31–32, 40].
- Bauxite residue ("red mud") and high-iron laterite wastes can be thermally processed; in combination with reduction or hydrometallurgical steps, they yield hematite/magnetite concentrates and enhance filtrability.[57].
- Bauxite residue ("red mud") and high-iron laterite wastes can be thermally treated; when followed by reduction or hydrometallurgical steps, they yield hematite/magnetite concentrates along with enhanced filtrability. [57].

Figure 7 illustrates the step-by-step process of thermal conditioning for goethitic materials, highlighting how temperature ranges align with process objectives and equipment choices. Each stage depicts a progressive change in the feed material: starting with moisture removal through drying, then transitioning to controlled dehydroxylation to convert goethite into hematite, and concluding with annealing or calcination to stabilize the structure and enhance mechanical strength. An optional magnetization roasting stage is included when magnetite production is required for further beneficiation or direct reduced iron (DRI) applications [2, 3, 27].

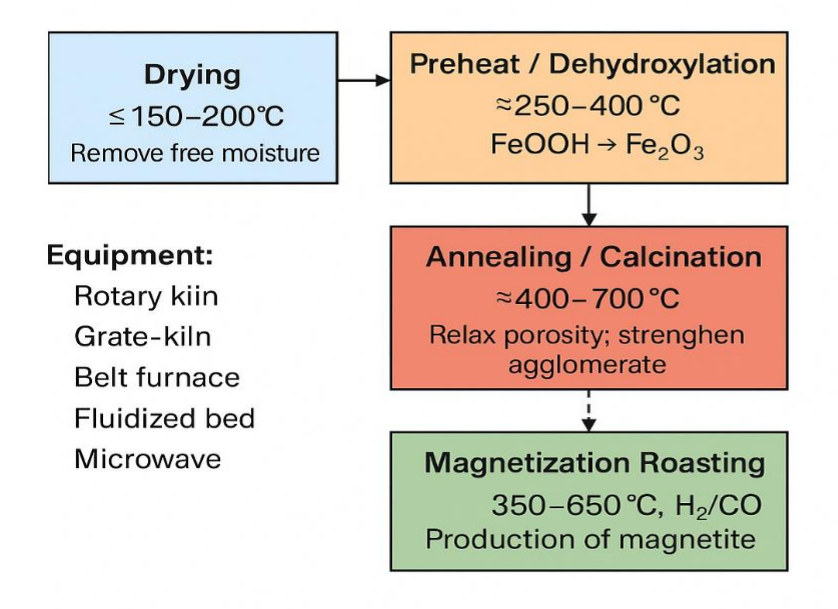


Figure 7. Thermal routes

Operational targets:

- Remove combined water before densifiction
- Avoid over-sintering Control atmosphere (inert/oxidizing or reducing)

Operational targets:

 Ramage combined water before densification The figure highlights the significance of managing atmosphere and operational goals. Precise regulation of gas composition and water vapor partial pressure is essential to prevent rehydration, over-sintering, or accidental reduction, as these issues can impair efficiency and lower product quality. This control becomes even more critical in sophisticated systems such as fluidized-bed reactors and microwave-assisted heating, which offer improved heat transfer and more precise process regulation [11, 12, 56].

The flowchart illustrates that traditional equipment, including rotary kilns and grate-kiln systems, remains prevalent in large-scale operations due to their durability and high throughput. Meanwhile, emerging technologies such as microwaves and hybrid systems offer potential improvements in energy efficiency and reduced carbon emissions [60, 62, 74].

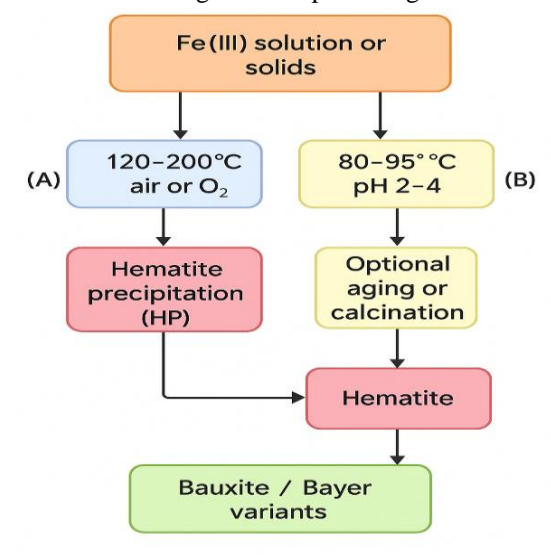
5.2. Hydrometallurgical processes

Two primary pathways are predominant:

- (A) Hematite precipitation (HP) at high temperatures occurs when Fe(III) dissolves or oxidizes in acidic solutions—such as zinc sulfate circuits—or is released from solids, then hydrothermally precipitates as hematite at approximately 120–200 °C in the presence of air or oxygen. HP results in dense, low-water hematite with favorable settling and filtration qualities, helping to minimize sodium and sulfate co-precipitation common in jarosite and goethite processes. Maintaining control over silicon and phosphate levels is crucial for purity and proper kinetic performance. [54–56, 59].
- (B) Goethite/Jarosite pathways, with optional aging to convert to hematite (G→H). Under milder conditions (around 80–95 °C; pH 2–4), Fe(III) precipitates as goethite or jarosite for iron removal. Subsequently, hydrothermal aging or low-temperature calcination transforms these into hematite. These approaches are standard when sulfate management and alkali budgets are priorities or when integration with Bayer-type liquors is required. Adjusting pH, Eh, and seed controls influences induction time and particle size. [12, 58, 59].

Bauxite/Bayer variants: In alumina production, Alsubstituted goethite in gibbsitic bauxites transforms at low to moderate temperatures and can be directed toward hematite formation, maximizing alumina extraction; alkaline chemistry alters the dehydroxylation energy and nucleation pathway. [12].

Figure 8 depicts two primary hydrometallurgical approaches for extracting iron and producing hematite.



Hydrometallurgical routes

Figure 8. Hydrometallurgical routes

Pathway A offers higher product quality with fewer impurities and less co-precipitation, but it requires more energy, making it less suitable for low-value streams [54,55]. In contrast, Pathway B, which operates at lower temperatures and costs, is common in integrated hydrometallurgical processes; however, it produces intermediate solids that need further processing [58,59].

The Bauxite/Bayer process highlights opportunities to combine iron removal with alumina recovery, aligning with circular economy objectives [12, 57]. Future developments should aim to optimize energy efficiency and impurity control, while also incorporating low-carbon energy sources to meet sustainability goals [74, 77, 78].

5.3. Hybrid routes (wet plus thermal))

Hybrid schemes selectively precipitate Fe(III) as ferrihydrite or goethite at pH 2–4 or If the grade is \geq 12, age the material to manage impurities and morphology before calcining it at 300–450 °C to produce hematite. This method separates solution chemistry processes—like controlling Si/P/Al and capturing trace metals—from the final densification and phase purification steps. Hybrids can lower energy consumption compared to high-temperature, long-duration kiln firing while still producing pigment.

Figure 9 illustrates the hybrid (wet + thermal) process for removing iron and producing hematite. Initially, Fe(III) is selectively precipitated as ferrihydrite or goethite under specific pH conditions (2–4 or ≥12). These precipitates are then aged to enhance particle morphology and control impurities, including trace metals such as Si, P, and Al. The final step involves thermal calcination at 300–450 °C, converting the intermediates into dense hematite. This method separates the solution chemistry control from the densification stage, resulting in high-quality products suitable for industrial applications such as pigments.

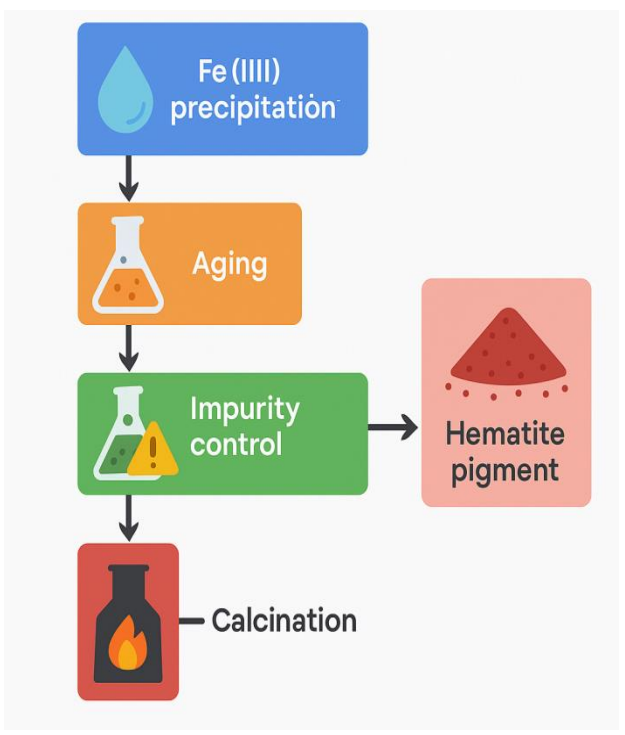


Figure 9. Hybrid routes.

Hybrid routes capitalize on the advantages of hydrometallurgical selectivity and thermal stability, thereby reducing total energy consumption compared to conventional high-temperature techniques. This method, which separates precipitation from calcination, enhances impurity control and particle morphology, resulting in higher-purity hematite and more efficient processing [56,59]. Nonetheless, it requires meticulous regulation of pH and redox conditions, adding to operational complexity, and managing intermediates between wet and thermal stages can boost capital expenses.

Despite these challenges, hybrids remain highly relevant for sustainable iron processing, as they reduce CO₂ emissions and support the valorization of by-products, such as pigments or trace metal concentrates [74, 77, 78]. Future work should aim to intensify the process and incorporate renewable energy or electrified heating to minimize environmental impact further [74, 76].

6. Industrial applications

6.1. Iron-ore beneficiation

Goethite-rich feeds benefit from a staged thermal conditioning process that first removes free and bound water, then transforms FeOOH into Fe2O3 prior to high-load agglomeration. Modern sinter and pellet facilities usually incorporate drying to 150-200 °C), (up preheating/dehydroxylation (around 250-400 °C), and annealing (about 400-700 °C) within a controlled atmosphere to prevent re-hydroxylation and over-sintering. This method reduces fuel consumption downstream by limiting endothermic dehydroxylation in the blast furnace or DRI unit, enhances bed permeability, and stabilizes strength properties. Field and pilot tests indicate that pore formation during

preheat substantially affects heat transfer and mechanical qualities, prompting cycle design modifications based on ore LOI and goethite content [11, 23–25, 31–32, 60–62].

Optional magnetization roasting at 350–650 °C in H₂/CO (R2) is becoming more common when the aim is magnetic separation or direct reduced iron (DRI). This process benefits from the quicker reduction rates of porous hematite and magnetite versus dense grains [26, 27, 33, 35–36,40].

6.2. Industrial residues

Goethite-rich residues such as bauxite residue (red mud), zinc hydrometallurgy liquors, and AMD sludges can be valorized by converting Fe(III) into filterable hematite or magnetite. In red mud, thermal or hydrochemical FeOOH to Fe₃O₄/Fe₂O₃ pathways enable Fe recovery and improve solid–liquid separation of the remaining matrix [14,57]. In zinc processes, two main hydrometallurgy routes dominate: (i) direct hematite precipitation at 120–200 °C in oxidizing autoclaves, producing dense, low-water solids with good settling and filtration; and (ii) goethite/jarosite precipitation at 80–95 °C (pH \approx 2–4) for iron removal, followed by hydrothermal aging or low-temperature calcination to hematite when sulfate and alkali budgets require (section 6.2).

Recent research has shown that hydrothermal conversion effectively transforms jarosite into hematite, resulting in recyclable, low-impurity products that aid process retrofits in sulfate circuits [58–59, 63]. In addition to base-metal streams, stepwise hydrothermal separations that precipitate Fe as hematite from complex sludges enhance the recovery of valuable metals such as Zn and produce an Fe₂O₃ by-product suitable for pigments or as feedstock for blending [68].

6.3. Pigments and advanced materials

Synthetic hematite $(\alpha\text{-Fe}_2O_3)$ serves as a primary red pigment due to its thermal and chemical stability. Its hue can be tuned by altering size, shape, or dopants, and it is compatible with ceramic glazes and architectural coatings. Microwave-assisted precipitation can lower the temperature required to transform goethite into hematite and reduce processing time. This facilitates pigment production from FeSO₄ residues via waste-to-pigment techniques, which allow easy filtration and result in high BET surface areas [64].

Al-modified hematite/alumina composites used in highvalue ceramics yield bright yellowish-red hues with strong thermostability; adding silica coatings improves mechanical durability and color retention, which is beneficial for porcelain stoneware and sanitary ware [67].

Hematite nanostructures play a key role in catalysis and functional materials as redox-active supports and photocatalysts, also serving in environmental cleanup. Recent reviews highlight the relationships between synthesis, structure, and properties that inform pigment and catalyst manufacturing strategies from goethitic sources [19, 65].

7. CAPEX and OPEX

7.1. Scope and boundaries

We determine costs at both the unit-operation and flow sheet levels—thermal, hydromet HP, $G \rightarrow H$, or hybrid. Unless specified otherwise, OPEX includes energy, reagents, consumables, maintenance, labor, waste management, and by-product credits; CAPEX encompasses core equipment, auxiliaries, utilities, installation, and controls/integration. We suggest reporting normalized KPIs such as GJ per ton of Fe (or per ton of dry feed), kWh per ton of water removed, tons of CO_2 per ton of Fe, and US dollars per ton of product [61, 62, 78].

7.2. Thermal processes (drying, followed by preheating/dehydroxylation, then annealing; magnetization roasting is optional)

CAPEX drivers encompass furnace selection (such as grate-kiln, rotary kiln, belt, or fluidized bed), gas handling (including off-gas condensation and dew-point regulation), and instrumentation (monitoring dew point, O₂ levels, and rapid mineralogy analysis). Fluidized beds involve additional CAPEX for distributors and air systems but can decrease overall footprint due to enhanced heat and mass transfer [60, 62]. Electrified preheaters and microwave systems require power delivery and shielding; however, they can reduce fluegas treatment expenses [56,74].

OPEX drivers include thermal duties such as heating solids, evaporating free water, and dehydroxylating FeOOH to Fe₂O₃ (an endothermic process). Additionally, they involve the operation of fans/draft systems and dust control measures [61,62]. Optional R2 magnetization adds reductants like H₂/CO and humidity regulation, providing advantages like magnetic upgrading and DRI compatibility. These benefits can reduce overall costs related to separation and downstream ironmaking processes [26, 27, 33, 35–36, 40].

7.3. Hydrometallurgical routes

(A) Hematite precipitation (HP, 120–200 °C, air/O₂).

CAPEX includes autoclaves (pressure vessels), oxygen/air compression, seed handling, and hot solid—liquid separation. OPEX covers steam/electricity for heating and agitation, oxygen, seeding/neutralization, and filtration media. The benefit stems from dense, low-water hematite, which provides better settling and filtration, thereby reducing

downstream dewatering OPEX compared to jarosite/goethite precipitates [54,55,58].

(B) Goethite/jarosite at 80–95 °C with aging or low-temperature calcination (G→H).

CAPEX involves atmospheric tanks, pH control, filters, and optionally a small calciner or aging reactor. [78].

7.4. Hybrid and low-carbon options

Hybrid thermal-hydromet (pre-dry \rightarrow hydromet HP or G \rightarrow H \rightarrow low-T anneal) can lower peak temperatures and flue-gas loads while achieving the desired morphology and density. Low-carbon strategies include hydrogen-assisted stages, electrified heat, and heat integration (off-gas condensation/steam reuse). Their economics depend on energy and H₂ prices, as well as site utilities; integrating with DRI/EAF enhances value capture [56, 60–62, 74, 76–79].

7.5. Major cost levers and sensitivities

- Feed properties such as LOI, goethite fraction, particle size/crystallinity, and Al–Si–P substitutions affect the R1 window and gas demand (energy/time) [12,18,24,31].
- Humidity control: Elevated p(H₂O) extends R1 and raises fuel consumption; upgrading condensers and ID fans often yields quick benefits [61,62].
- Product specs & credits: Dense hematite that meets pigment/sinter-feed specs increases revenue or decreases blending costs [30,64–65,67–68].
- Fluidized beds scale well for fines, while kilns are appropriate for mixed feeds and brownfield retrofits [60,62].
- Electrification & H₂: OPEX becomes more sensitive to electricity and H₂ prices; emissions decrease when lowcarbon power is accessible [56,74,76].

7.6. Reporting template (recommended)

CAPEX includes equipment, installation, utilities (such as gas treatment, oxygen/ H_2 , power), controls, EPC, and contingency. OPEX covers energy (in GJ/t), reagents and consumables, maintenance costs (as a percentage of the installed cost), labor, waste management, and credits from by-products.

KPIs: GJ per ton of feed; kWh per ton of water removed; tCO₂ per ton of iron; US dollars per ton of Fe₂O₃ (or Fe in DRI); filtrability index; pellet CCS/sinter TI.

Table 4 outlines the primary CAPEX and OPEX drivers across three processing methods: thermal, hydrometallurgical, and hybrid/low-carbon technologies, while also highlighting key cost sensitivities.

Table 4. Consolidated table - CAPEX and OPEX

. Section	Key Items	Description / Examples	Relevant KPIs
Thermal Routes	CAPEX	Furnace type (grate, rotary, fluidized bed), off-gas treatment systems, advanced instrumentation (O ₂ , dew point, fast mineralogy).	GJ/t dry feed, kWh/t H ₂ O removed.
	OPEX	Heating of solids, water evaporation, dehydroxylation,	tCO ₂ /t Fe

. Section	Key Items	Description / Examples	Relevant KPIs
		fan and draft consumption, dust control, reagents for magnetization roasting.	
Hydrometallurgical Routes	CAPEX	Autoclaves, O ₂ compression systems, atmospheric tanks, filters, aging reactors.	US\$/t Fe ₂ O ₃
	OPEX	Steam and electricity, oxygen, acids/bases, neutralization, filtration media.	Filtrability index
Hybrid & Low-Carbon	CAPEX	Heat integration systems, electrified heating, H ₂ infrastructure.	Emissions reduction (tCO ₂ /t)
	OPEX	Electricity and H ₂ as major cost drivers, savings from heat recovery.	Pellet CCS / Sinter TI
Cost Sensitivities	-	LOI, goethite fraction, particle size, $p(H_2O)$ control, scale, and plant layout.	-

Thermal routes remain CAPEX-intensive but provide good scalability and reliability. Meanwhile, hydrometallurgical options offer higher selectivity but incur higher OPEX due to reagent and energy costs [54,55,59]. Hybrid and low-carbon systems could lower long-term OPEX and environmental impact, but they require higher initial CAPEX and more advanced technology [74,76,77].

For sustainable process design, optimizing trade-offs requires a system-level approach that balances economics and environmental impact, especially during the transition to decarbonized iron production [74,77,78]. It analyzes CAPEX (blue) and OPEX (red) sensitivities across six key factors shaping industrial process design: Furnace Type, Humidity Control, Product Specifications, Electrification/H₂ Integration, Scale & Layout, and Thermal Energy Demand.

Figure 10 shows a radar chart depicting the sensitivity of CAPEX (blue line) and OPEX (red line) across six key factors influencing process design and economic viability.

CAPEX primarily relies on Furnace Type, Scale, and Layout, focusing on the upfront costs for equipment and infrastructure.

Humidity Control and Thermal Energy Demand have more influence on OPEX because these factors directly affect ongoing operational costs, such as energy use and process stability.

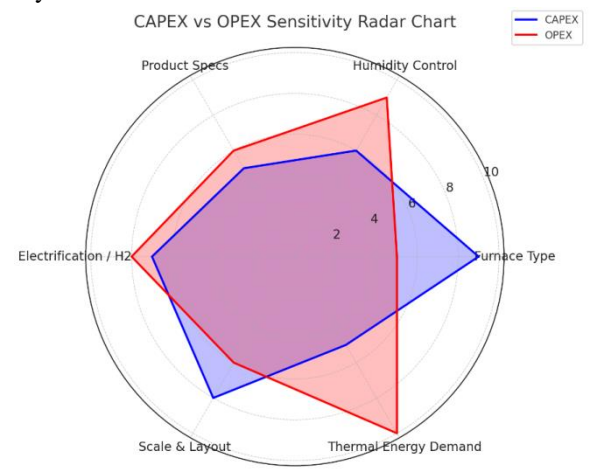


Figure 10 CAPEX vs OPEX Sensitivity Radar Chart

This comparison highlights the strategic trade-off between capital investments and operational considerations.

- Investing heavily in advanced furnace technologies can decrease operational costs through improved energy efficiency and reduced maintenance expenses, but it is essential to carefully assess the payback period [61,74].
- The prominence of Thermal Energy Demand in OPEX highlights the significance of energy efficiency and process optimization, particularly in areas facing increasing energy prices or decarbonization challenges [74,76].
- Humidity control greatly influences operational costs, particularly in hydrometallurgical and drying processes, as excess moisture increases energy consumption and decreases process reliability [11,56].

To ensure long-term sustainability, integrating electrification with hydrogen technologies can reduce OPEX linked to fossil fuel dependence, although it may initially increase CAPEX because of infrastructure and technology development expenses [60, 76, 77].

This chart ultimately serves as a decision-making aid that balances short-term investment constraints with long-term operational savings and environmental impact, supporting the development of economically viable and sustainable process designs.

8. Characterization techniques

This section outlines what each technique uncovers, how to use them for goethite-to-hematite transformations, and typical mistakes encountered with natural ores and industrial residues.

8.1. X-ray diffraction (XRD)

During the goethite-to-hematite transformation, XRD enables the detection and quantification of phases like goethite (α -FeOOH), hematite (α -Fe2O₃), ferrihydrite, jarosite, and magnetite. This method is crucial for monitoring thermal, hydrometallurgical, and hybrid processes, providing valuable information on reaction kinetics, crystallinity, and phase purity [18, 27, 28].

High-resolution XRD combined with Rietveld refinement allows for the identification of minor phases and lattice substitutions, like aluminum or silicon incorporation in goethite or hematite, which affect transformation behavior and properties of the final product [16,20]. Moreover, in situ XRD studies provide important insights into structural changes during heating or reduction, aiding the optimization of industrial processes [38,40,43].

Overall, XRD is a non-destructive and highly informative technique that delivers crucial data for process control and research, aiding the development of sustainable and efficient iron ore processing methods.

8.2. Mössbauer Spectroscopy (Fe)

Mössbauer spectroscopy differentiates oxidation and coordination states, such as Fe^{3+} versus Fe^{2+} , and distinguishes hematite sextets from goethite and ferrihydrite doublets, including superparamagnetic fractions. During heating, hyperfine parameters reveal dehydroxylation and topotactic reordering. Under reducing gases, they indicate the transient formation of Fe^{2+} and magnetite [33,40]. Recent reviews summarize protocols and common pitfalls, like magnetic relaxation in nano-hematite [69].

Good practice involves recording spectra at 300 K and low temperatures (4–80 K) to account for superparamagnetism, and ensuring that Mössbauer area fractions align with XRD quantification.

8.3. Thermal analysis (TG/DTG/DSC/DTA)

The TG/DTG/DSC profile shows mass losses and enthalpy changes associated with dehydroxylation (R1) and subsequent reduction steps (R2–R4). In goethitic ores, the main dehydroxylation usually occurs between 250–400°C, influenced by particle size, isomorphic substitutions (Al, Ga), and gas p(H₂O) [12,18,24]. Combining high-temperature DTA/DSC with magnetic susceptibility measurements helps distinguish endothermic R1 peaks from changes in magnetization, thereby improving the understanding of activation energies and mechanisms under relevant atmospheric conditions [44,72].

Good practice includes controlling gas flow and composition (pO_2 , pH_2O), calibrating buoyancy effects, and, when feasible, integrating analysis with evolved-gas techniques such as QMS or FTIR.

8.4. Electron microscopy (SEM/TEM) and correlative tools

SEM/TEM images reveal morphology, transient porosity, and topotactic textures like plates and lamellae, which affect filtration and agglomerate strength after R1. Insitu liquid-phase TEM has demonstrated dissolution–reprecipitation behavior and beam-induced radiolysis chemistry relevant to solution-mediated processes [50], as well as the anisotropic dissolution pathways of iron-oxide nanoparticles [73].

Good practice involves using representative crosssections (ion-milling) and carefully interpreting LP-TEM, especially when beam chemistry influences local redox processes.

8.5. Vibrational Spectroscopy (FTIR/Raman)

FTIR and Raman spectroscopy are used to identify structural OH groups, adsorbed water, and Fe-O vibrational modes. Goethite exhibits distinct OH absorption bands around 3.1-3.2 µm and bending modes near ~900 cm⁻¹, which indicate crystallinity and substitution effects. Conversely, hematite, with its corundum structure, is typically anhydrous and shows strong Fe-O modes. Recent experimental and DFT studies have associated vibrational signatures with magnetic exchange in α-FeOOH [70], with spectral changes reflecting crystallinity and composition in well-formed natural samples [71]. In systems containing organics or phosphates, ATR-FTIR coupled with the surrounding liquid allows for surface complexation monitoring, potentially shifting the dehydroxylation window and affecting the hydrogen peroxide (HP) versus G→H hydromet routes [17,70].

Good practice includes consistently drying and conditioning samples to avoid H₂O masking, utilizing ATR for surface-sensitive measurements, and cross-checking results with XRD or Mössbauer spectroscopy.

9. Challenges and Future Perspectives

Industrial scale-up faces challenges due to the heterogeneity of goethite-rich feeds, which vary in LOI, Al—Si—P substitutions, and particle size. This variability complicates heat and mass transfer, off-gas humidity management, and consistent dehydroxylation in large beds or kilns. Transitioning from lab or bench-scale to larger systems like grate—kiln, rotary-kiln, or fluidized-bed reveals issues such as microcracking, pore collapse, and over-sintering, which can weaken strength, reduce filtrability, and increase energy use. Electrification methods—resistive, induction, microwave—are promising for process heat but present challenges like high capital costs, material compatibility issues, and grid-carbon constraints when retrofitting plants. Therefore, detailed techno-economic analysis and control codesign are crucial.

Integrating the circular economy involves valorizing iron-rich residues such as red mud, jarosite/goethite precipitates, and lateritic tailings by directing them toward hematite/magnetite production and then into DRI/EAF processes. This strategy helps close material loops and reduces residue storage risks. However, LCA indicates that burden shifting could occur if chemicals, energy, and transportation are not managed efficiently. High-value pathways like hydrothermal hematite precipitation and hydrogen-assisted processes, including plasma reduction, are promising but require careful control of impurities (e.g., Si, P,

alkalis) and effective solid—liquid separation to be commercially viable.

Developing low-carbon processes involves hydrogen-based direct reduction (DR), magnetization roasting with low-carbon reductants, and electrified heating, including hybrid microwave pre-heats. These techniques can greatly reduce Scope-1 emissions when water vapor (H₂O/H₂) and pO₂ are carefully managed to avoid FeO bottlenecks and over-sintering. System analyses indicate that achieving deep decarbonization also relies on the upstream electricity and hydrogen footprints, as well as combining residue valorization with DRI/EAF processes. [33, 40, 56, 60–62, 76–79].

AI-enabled sensing, control, and digitalization are rapidly progressing. Key advances include soft sensors for predicting moisture, dew-point, burn-through-point, and mode recognition during sintering and roasting; integrating computer vision with probabilistic and machine learning models enhances early-warning systems and refines set-points. Digital twins streamline scale-up processes and facilitate 'what-if' analyses for energy consumption and emissions. However, challenges remain in making sensors robust against domain shifts, providing understandable control actions within safety limits, and developing reliable online sensors for gas humidity, as well as phase or porosity monitoring in hot zones.3].

10. Conclusions

Summary of progress (2020–2025).

Over the past five years, research has clarified how goethite transforms into hematite, identifying the topotactic dehydroxylation temperature (~250-400 °C) as influenced by particle size and Al/Ga substitution. Variations in density, filtrability, and strength are explained by vacancy filling, transient porosity, and coalescence. Enhanced thermodynamic and kinetic maps now relate T-time-pO₂p(H2O), while operando techniques such as synchrotron XRD, thermal analysis with magnetic measurements, and insitu TEM/IR/Raman enable real-time observation of transformation pathways—distinguishing solid-solid from dissolution-precipitation. In industry, staged drying, preheating, and annealing are standard for goethitic feeds. Magnetization roasting (H₂/CO, 350-650 °C) provides a flexible option for beneficiation and DRI production. Hydrometallurgy relies on primary methods like hematite precipitation (HP, 120-200 °C, oxidizing) goethite/jarosite precipitation (80-95 °C), with aging or lowtemperature calcination converting materials into hematite. Additionally, electrified heat sources such as microwave and induction heating are increasingly used. AI-assisted control is advancing from pilot projects toward early commercial deployment.

Industrial mportance.

- Iron-ore beneficiation involves removing structural water and pre-treating hematite to enhance bed permeability, reduce fuel consumption during sintering and pelletizing, and stabilize mechanical properties. An optional conversion of Fe₂O₃ to Fe₃O₄ allows magnetic upgrading and facilitates DRI integration.
- Industrial residues such as red mud and sulfate-circuit iron streams are increasingly being sent to dense, lowwater hematite or magnetite. This enhances dewatering and enables the recovery of by-product Fe, while also protecting the value chains of Al, Ti, and Zn.
- Pigments and advanced materials: Custom hematite (size, shape, dopants) enables applications in red pigments, ceramics, and catalysis; waste-to-pigment methods are possible if purity and particle design are preserved.

Gaps and potential directions for future research.

- 1. Standardized reporting of dehydroxylation kinetics covers particular p(H₂O)/pO₂ ratios, particle features, and impurity types such as Si, P, and alkalis.
- Scale-bridging operando diagnostics and inline sensors (dew point, fast XRD/LIBS/IR) to connect microstructure with plant set points.
- Implement process intensification techniques, such as fluidized beds and forced vapor removal, to manage thick beds and fine feeds. This helps prevent over-sintering and reduces R1 residence times.
- Validated models and digital twins (combining firstprinciples and machine learning) for model predictive control of temperature ramps, gas composition, and bed depth amid changing feed conditions.
- Low-carbon pathways: conduct comprehensive TEA/LCA for electrified heating and H₂-assisted processes, integrating with DRI/EAF and residue valorization.
- Product performance assurance involves guaranteeing long-term stability and adherence to market standards for hematite and magnetite produced from residues, such as pigment grade, sinter feed, or cement additives.

References

- Page MJ, McKenzie JE, Bossuyt PM, Boutron I, Hoffmann TC, Mulrow CD, et al. The PRISMA 2020 statement: an updated guideline for reporting systematic reviews. BMJ. 2021;372:n71. https://doi.org/10.1136/bmj.n71
- Study on Magnetization Roasting Kinetics of High-Iron and Goethite-bearing Minerals. L Xie, et al. 2023. DOI:10.3390/pmc10533041? (full DOI: PMC10533041)

- Li M, Zhang H, Yang F, Chen T, Lu M, Yu H. XPS Investigation of Magnetization Reduction Behavior and Kinetics of Oolitic Hematite in Gas-Based Roasting. Minerals. 2024;14(5):462. https://doi.org/10.3390/min14050462
- Q Zhang, et al. Reaction behavior and non-isothermal kinetics of limonite and siderite in a SMR process: dehydration of goethite to hematite etc. 2023. Springer article. DOI:10.1007/s12613-022-2523-3
- Hu B, et al. Iron oxyhydroxide polytype (γ-, δ- and β-FeOOH) structures in substituted goethite/hematite systems enhancing element release. 2022. DOI available in article S0009254122004612
- 6. Adeoye AO, et al. Wet synthesis, characterization of goethite nanoparticles via coprecipitation... 2023. DOI from the article (S2666845923000235)
- 7. Study: Mineralogical Study of Low and Lean Grade Iron Ore Fines conversion behavior of goethite etc. 2022. DOI from GeoscienceWorld article 98(8):1159-??
- Ponomar VP, Gavryliv LI, Brik AB. Mineral and magnetic transformations of goethite-hematite low-grade iron ores under oxidative and reductive roasting. 2022-2023. DOI / Full-text via preprint / SSRNhttps://ssrn.com/abstract=4291929
- The PRISMA-S checklist: PRISMA-S is an extension to the PRISMA Statement for reporting literature search strategies in systematic reviews [10]. DOI:10.1186/s13643-020-01542-z
- 10. Furcas FE, Mundra S, Lothenbach B, et al. Transformation of 2-Line Ferrihydrite to Goethite at Alkaline pH \geq 13.0: kinetics etc. 2023. DOI:10.1021/acs.est.3c05260
- 11. Zhu DQ, Pan J, Pan X, Li C, Fan X. Moisture migration behavior of goethitic iron ore fines during drying process. Powder Technology. 2023;420:118387. https://doi.org/10.1016/j.powtec.2023.118387.
- Zhou G, Wang Y, Qi T, Zhou Q, Liu G, Peng Z, et al. Low-temperature thermal conversion of Al-substituted goethite in gibbsitic bauxite for maximum alumina extraction. RSC Advances. 2022;12:4162-4174. https://doi.org/10.1039/D1RA09013E.
- Tavares LM, Rabelo AA, Vieira JÁ, Araújo AC, Vieira CMF. Effect of goethite content on the processing behavior and metallurgical performance of iron ore pellets. Minerals Engineering. 2021;171:107088. https://doi.org/10.1016/j.mineng.2021.107088.
- Zhu J, Li H, Sun Y, Zhang Y, Chen X, Liu Q. Recovery of iron from red mud by reduction roasting–magnetic separation: role of goethite and hematite phases. *Journal of Cleaner Production*. 2022;332:130040. DOI:10.1016/j.jclepro.2021.1300

- 15. Abrashev MV, Pashkova A, Hadjiev VG, et al. Raman spectroscopy of α -FeOOH (goethite): Lattice dynamics and OH vibrations. J Appl Phys. 2020;127:205108. doi:10.1063/5.0006352.
- 16. Filippov LO, François M, Drouet C, Vantelon D, Proux O, Lassin A, et al. Molecular models of hematite, goethite, kaolinite and quartz: Surface terminations, ionic interactions, nano-topography and water coordination. Colloids Surf A Physicochem Eng Asp. 2022;650:129585. doi:10.1016/j.colsurfa.2022.129585.
- 17. Yi S, Chen X, Cao X, Yi B, He W. Influencing factors and environmental effects of interactions between goethite and organic matter: A critical review. Front Environ Sci. 2022;10:1023277. doi:10.3389/fenvs.2022.1023277.
- 18. Chen SA, Heaney PJ, Post JE, Eng PJ, Stubbs JE. Hematite/goethite ratios at pH 2–13 and 25–170 °C: A time-resolved synchrotron X-ray diffraction study. Chem Geol. 2022;606:120995. doi:10.1016/j.chemgeo.2022.120995.
- 19. Li Y, Dang J, Ma Y, Ma H. Hematite: A good catalyst for the thermal decomposition of energetic materials and the application in nano-thermite. Molecules. 2023;28(5):2035. doi:10.3390/molecules28052035.
- 20. Buist A, Rivard C, Davranche M, Vantelon D, Hanna K, et al. Impact of aluminium and gallium substitutions on the ferrihydrite and goethite structure: Consequences for rare earth element adsorption and complexation. Chem Geol. 2024;667:122312. doi:10.1016/j.chemgeo.2024.122312
- 21. Yan S-F, Li L, Yuan M, Santosh M. High-pressure and high-temperature behaviour of α-FeOOH and ε-FeOOH: a geological perspective. Crystallography Reviews. 2025;30(...):... doi:10.1080/0889311X.2025.2470143.
- 22. Esdaille SS, Drozd V, Durygin A, Li W, Chen J. Spectroscopic evidence for the α-FeOOH-to-ε-FeOOH phase transition: insights from high-pressure and high-temperature Raman spectroscopy. Crystals. 2025;15(9):782. doi:10.3390/cryst15090782.
- 23. Chen P, Zhou X. A Study on the Influence of Drying and Preheating Parameters on the Roasting Properties of Limonite Pellets. *Minerals*. 2024;14(2):166. doi:10.3390/min14020166.
- 24. Pereira IJUV, Hild CH, Ignatyeva J, Kleebe H-J. Batch Sintering of FeO·OH and Fe₂O₃ Blends: Chemical and Microstructural Evolution. *Metals*. 2024;14(5):598. doi:10.3390/met14050598.
- 25. Wang J, Ma P, Meng H, Cheng F, Zhou H. Investigation on the evolution characteristics of bed porous structure during iron ore sintering. *Particuology*. 2023;74:35–47. doi:10.1016/j.partic.2022.05.005.

- 26. Heidari M, Nemati R, Movahedi M, Ghasemi M. A Review on the Kinetics of Iron Ore Reduction by Hydrogen. *Materials*. 2021;14(24):7540. doi:10.3390/ma14247540.
- 27. Kukkala PC, Kumar S, Nirala A, Khan MA, Alkahtani MQ, Islam S. Beneficiation of Low-Grade Hematite Iron Ore Fines by Magnetizing Roasting and Magnetic Separation. *ACS Omega*. 2024;9(7):7634–7642. doi:10.1021/acsomega.3c06802.
- 28. Wang G, Zhang J, Liu Z, Tan Y, Wang Y. Cracking and Microstructure Transition of Iron Ore Containing Goethite in Fe–C Melt Based on the HIsmelt Process. *Minerals*. 2023;13(3):448. doi:10.3390/min13030448.
- 29. Chen SA, Heaney PJ, Post JE, Fischer TB, Eng PJ, Stubbs JE. Superhydrous hematite and goethite: A potential water reservoir in the red dust of Mars? *Geology*. 2021;49(11):1343–1347. doi:10.1130/G48929.1.
- Valášková M, Leštinský P, Matějová L, Klemencová K, Ritz M, Schimpf C, et al. Hematites Precipitated in Alkaline Precursors: Comparison of Structural and Textural Properties for Methane Oxidation. *Int J Mol Sci*. 2022;23(15):8163. doi:10.3390/ijms23158163
- 31. Prusti P, Barik K, Dash N, Biswal SK, Meikap BC. Effect of limestone and dolomite flux on the quality of pellets using high LOI iron ore. *Powder Technol*. 2021;379:154–164. doi:10.1016/j.powtec.2020.10.063.
- 32. Cavaliere P, Sadeghi B, Dijon L, Laska A, Koszelow D. Three-dimensional characterization of porosity in iron ore pellets: A comprehensive study. *Minerals Engineering*. 2024;213:108746. doi:10.1016/j.mineng.2024.108746.
- 33. Miškovičová Z, Vontorová J, Průša F, Knaislová A, Kubíček J, et al. An overview analysis of current research status in iron oxides reduction by hydrogen. *Metals*. 2024;14(5):589. doi:10.3390/met14050589.
- 34. Wang K, Zhang X, Fu M, Chen M, Xu Z, Xu J. Potential—pH diagrams considering complex oxide solution chemistry. *npj Mater Degrad*. 2020;4:35. doi:10.1038/s41529-020-00141-6.
- 35. He J, Goprinska M, Yang G, Leion H. Reduction kinetics of compact hematite with hydrogen between 600 and 1000 °C. *Metals*. 2023;13(3):464. doi:10.3390/met13030464.
- 36. Fradet Q, Neumann J, Roeb M, Sattler C. Thermochemical reduction of iron oxide powders with hydrogen: review of selected thermal analysis studies. *Thermochim Acta.* 2023;726:179552. doi:10.1016/j.tca.2023.179552.
- 37. Robinson TC, Gorski CA, Griffin JS, Rosso KM, Tratnyek PG. Redox potentials of magnetite suspensions

- under reducing conditions. *Environ Sci Technol*. 2022;56(24):17146–17155. doi:10.1021/acs.est.2c05196.
- 38. Chen SA, Heaney PJ, Post JE, Eng PJ, Stubbs JE. Vacancy infilling during the crystallization of Fedeficient hematite: an *in situ* synchrotron X-ray diffraction study of nonclassical crystal growth. *Am Mineral*. 2023;108(9):1720–1731. doi:10.2138/am-2022-8379.
- 39. Geymond U, Mathieu I, Monnin C, Truche L, Levy S, et al. Reassessing the role of magnetite during natural hydrogen generation. *Front Earth Sci.* 2023;11:1169356. doi:10.3389/feart.2023.1169356.
- Zender L, Waidhauser T, Dolle C, Müller H, Asylbekov S, et al. Following the structural changes of iron oxides during hydrogen reduction: operando insights and implications for industrial decarbonization. *ChemSusChem*. 2024;17:e202401045. doi:10.1002/cssc.202401045
- 41. arley KA, Monteiro HB, Vasconcelos PM, Waltenberg K. Dehydration of goethite during vacuum step-heating and implications for He retentivity characterization. *Chemical Geology*. 2024;663:122254. doi:10.1016/j.chemgeo.2024.122254.
- 42. Kurniawan A, Saito G, Nomura T, Akiyama T. Faster generation of nanoporous hematite ore through dehydration of goethite under vacuum conditions. *ISIJ International*. 2021;61(1):493–497. doi:10.2355/isijinternational.ISIJINT-2020-403.
- 43. Leerhoff P, Brouwer JC, Armaki AM, Zeilstra C, Meijer K, van der Stel J, et al. Characterisation of varying iron ores and their thermal decomposition kinetics under HIsarna ironmaking conditions. *Metals*. 2024;14(11):1271. doi:10.3390/met14111271.
- 44. Doctor R, Feinberg JM. Differential thermal analysis using high-temperature susceptibility instruments. *J Geophys Res: Solid Earth.* 2022;127:e2021JB023789. doi:10.1029/2021JB023789.
- 45. Krzemnicki MS, Lefèvre P, Zhou W, Braun J, Spiekermann G. Dehydration of diaspore and goethite during low-temperature heating as criterion to separate unheated from heated rubies and sapphires. *Minerals*. 2023;13(12):1557. doi:10.3390/min13121557.
- 46. Notini L, Schulz K, Kubeneck LJ, Grigg ARC, Rothwell KA, Fantappiè G, et al. Coexisting goethite promotes Fe(II)-catalyzed transformation of ferrihydrite to goethite. *Environ Sci Technol*. 2022;56(17):12723–33. doi:10.1021/acs.est.2c03925
- Lázaro I, González-López J, Aparicio P, Largo-Arcos J, Herrero M, Parras M, et al. Thermal transformation of natural schwertmannite in the presence of chromium. *Minerals*. 2022;12(6):726. doi:10.3390/min12060726.

- 48. Kim HJ, Kim Y. Schwertmannite transformation to goethite and the related mobility of trace metals in acid mine drainage. *Chemosphere*. 2021;269:128720. doi:10.1016/j.chemosphere.2020.128720.
- 49. Ryu J-G, Kim Y. Mineral transformation and dissolution of jarosite coprecipitated with hazardous oxyanions and their mobility changes. *J Hazard Mater*. 2022;427:128283. doi:10.1016/j.jhazmat.2022.128283.
- 50. Couasnon T, Denizot B, Simoes M, Troadec D, Gatel C, Bechelany M, et al. Goethite mineral dissolution to probe the chemistry of radiolytic water in liquid-phase TEM. *Adv Sci.* 2023;10(31):e2301904. doi:10.1002/advs.202301904.
- 51. Mørch MI, Thomas-Hunt J, Laursen AP, Jensen KH, Kehres J, Michels N, et al. Oriented nanomagnets originating from topotactic and pseudomorphic reactions. *Chem Mater*. 2024;36(4):1528–39. doi:10.1021/acs.chemmater.3c02616.
- 52. Sassi M, Rosso KM. Ab initio evaluation of solid-state transformation pathways from ferrihydrite to goethite. ACS Earth Space Chem. 2022;6(3):800–9. doi:10.1021/acsearthspacechem.2c00026. Publicações ACS
- 53. Schulz K, ThomasArrigo LK, Rothwell KA, Grigg ARC, Kaegi R, Kretzschmar R. Iron oxyhydroxide transformation in a flooded rice paddy field: the role of phosphate and direct soil contact. *Environ Sci Technol*. 2024;58(19):—. doi:10.1021/acs.est.4c01519.
- 54. Li C, Li Z, Liu X, Jeřábek K, Komárek P. Hydrothermal precipitation of hematite from the model solution of zinc hydrometallurgical extraction. *Int J Chem React Eng.* 2024;22(7). doi:10.1515/ijcre-2023-0073.
- 55. Peng X, Zhou X, Yang H, Guo X, Zhu Y, Shao H, et al. Dissolution behavior of hematite in H₂SO₄ solution: implications for the hematite process. *Miner Eng.* 2024;215:108811. doi:10.1016/j.mineng.2024.108811.
- Chen J, Li X, Gao L, Guo S, He F. Microwave treatment of minerals and ores: heating behaviors, applications, and future directions. Minerals. 2024;14(3):219. https://doi.org/10.3390/min14030219.
- 57. Shoppert A, Baba Yepnest I, Akcil A, Akdogan G. Highiron bauxite residue (red mud) valorization using hydrochemical conversion of goethite to magnetite.

 Materials. 2022;15(23):8423. https://doi.org/10.3390/ma15238423
- 58. Hoeber L, Steinlechner S. A comprehensive review of processing strategies for iron precipitation residues from zinc hydrometallurgy. *Cleaner Eng Technol.* 2021;4:100214. doi:10.1016/j.clet.2021.100214.
- 59. Formoso P, Barriga O, Navarro-Blasco I, Guerrero A. Jarosites: formation, structure, reactivity and

- environmental implications. *Metals* (*Basel*). 2022;12(5):802. doi:10.3390/met12050802.
- 60. Wolfinger T, Reinmöller M, Alobaid F, Epple B. Using iron ore ultra-fines for hydrogen-based fluidized-bed direct reduction—challenges and opportunities. Metals. 2022;12(6):996. https://doi.org/10.3390/met12060996.
- 61. Na H, Kim S, Kim J, Wang Y, Zhang H. Theoretical energy consumption analysis for sustainable practices in the iron and steel industry. Metals. 2024;14(5):563. https://doi.org/10.3390/met14050563.
- 62. Bojanovský J, Adamus J, Čarnogurská M, Mikuš R. Rotary kiln, a unit on the border of the process and energy industry—current state and perspectives. *Sustainability*. 2022;14(21):13903. doi:10.3390/su142113903.
- 63. Xing Y, Wei C, Deng Z, Li X, Li M. Alternative to the jarosite process:transforming jarosite into recyclable hematite by a hydrothermal method. *Sci Rep.* 2024;14:24490. doi:10.1038/s41598-024-75857-5.
- 64. Splinter K, Machowiak D, Lendzion-Bieluń Z. Microwave-reactor-based preparation of red iron oxide pigment from waste iron sulfate. *Materials*. 2023;16(8):3242. doi:10.3390/ma16083242.
- 65. Wan J, Li X, Wang W, Xu J, Wu W, Wang Z, *et al.* Advanced hematite nanomaterials for newly emerging applications. *Chem Sci.* 2023;14:6944–66. doi:10.1039/D3SC00180F.
- 66. Li Y, Wang F, Hou Y, Dong H, Liu X, Song X, et al. Precipitation of magnetite nanoparticles in situ for resource and energy saving in microfluidic-based Fe–Zn separation. Environ Sci Nano. 2024;11:606–17. doi:10.1039/D3EN00696D.
- 67. Hashimoto H, Kiyohara J, Isozaki A, Arakawa Y, Fujii T, *et al.* Bright yellowish-red pigment based on hematite/alumina composites with a unique porous disk-like structure. *ACS Omega.* 2020;5:4330–37. doi:10.1021/acsomega.9b04297.
- 68. Qu Z, Su T, Zhu S, Chen Y, Yu Y, Xie X, *et al.* Stepwise extraction of Fe, Al, Ca, and Zn: a green route to recycle raw electroplating sludge. *J Environ Manage*. 2021;300:113700. doi:10.1016/j.jenvman.2021.113700
- Wareppam SK, Chatterjee S, Dhar S, Naik AD. Mössbauer spectroscopic investigations for iron-oxide nanostructures: an overview. *Mater Res* (São Carlos). 2022;25:e20220244. doi:10.1557/s43578-022-00665-4.
- Sit PHL, Ganesh KJ, Bouville M. Vibrational spectra and magnetic exchange in goethite: coupling between lattice dynamics and magnetism. *Phys Chem Chem Phys*. 2023;25:22732–22743. doi:10.1039/D3CP01200J.

- Kaufhold S, Ufer K, Hein M, Götze N, Dohrmann R. A combined IR and XRD study of natural well crystalline goethites (α-FeOOH). *Acta Geochim*. 2022;41:794–810. doi:10.1007/s11631-022-00546-x.
- 72. Leerhoff P, Brouwer JC, Armaki AM, Zeilstra C, Meijer K, van der Stel J, *et al.*Characterisation of varying iron ores and their thermal decomposition kinetics under HIsarna ironmaking conditions. *Metals* (*Basel*). 2024;14(11):1271. doi:10.3390/met14111271.
- 73. Liu L, Liu Y, Lin J, Li T, Zhu W, Zheng H, *et al.* Understanding the mechanisms of anisotropic dissolution of iron oxide nanoparticles via in situ liquid-phase TEM. *Proc Natl Acad Sci USA*. 2023;120:e2101243120. doi:10.1073/pnas.2101243120.
- 74. Amber T, Aditya L, Brown S, et al. Electrifying industrial heat: A review of technology options, system integration, and decarbonization potential. Energies. 2023;16(19):6894. https://doi.org/10.3390/en16196894.
- 75. Xing Y, Wei C, Deng Z, Li X, Li M. Alternative to the jarosite process: transforming jarosite into recyclable hematite by a hydrothermal method. *Sci Rep.* 2024;14:24490. doi:10.1038/s41598-024-75857-5.
- 76. Tsiropoulos I, Ranzani A, van der Stel J, van den Boogaart K. Review of hydrogen-based direct reduction of iron ore technologies and integration with EAF. *Processes*. 2024;12(4):757. doi:10.3390/pr12040757.
- 77. Jovičević-Klug M, Hryha E, Nyberg E, et al. Green steel from red mud through climate-neutral hydrogen-plasma

- reduction. *Nature.* 2024;626:583–589. doi:10.1038/s41586-023-06901-z.
- 78. Ma Y, Navrotsky A, Ferrari B, et al. Life cycle assessment of pig iron production from bauxite residue in Europe. *J Ind Ecol.* 2023;27(6):1450–1464. doi:10.1111/jiec.13448.
- Hoeber L, Steinlechner S. Processing strategies for iron precipitation residues from zinc hydrometallurgy: a comprehensive review. *Cleaner Eng Technol*. 2021;4:100214. doi:10.1016/j.clet.2021.100214.
- Du S, Wu M, Chen L, Cao W, Pedrycz W. Operating-mode recognition based on clustering of time-series data for the iron-ore sintering process. *Control Eng Pract*. 2020;96:104297. doi:10.1016/j.conengprac.2020.104297.
- 81. Wang Z, Ma J, Wu L, et al. Prediction of sinter drum strength by optimized RBF neural network. *Ironmaking & Steelmaking*. 2023;50(8):947–956. doi:10.1080/03019233.2022.2096991.
- 82. Du S, Chen L, Wu M, Cao W, Pedrycz W. An intelligent decision-making strategy based on abnormal operating-mode forecasting for iron-ore sintering. *J Process Control.* 2020;96:57–66. doi:10.1016/j.jprocont.2020.11.001
- 83. Timperi M, Jussila J, Huiskonen J. Digital twins for environmentally sustainable and circular manufacturing: opportunities and challenges. *J Ind Inf Integr.* 2024;100:2428249. doi:10.1080/21693277.2024.2428249.